Microporous and Mesoporous Materials 184 (2014) 151–161

Contents lists available at ScienceDirect

Microporous and Mesoporous Materials

journal homepage: www.elsevier.com/locate/micromeso

Tuning the pore structure of plug-containing Al-SBA-15 by post-treatment and its selectivity for C_{16} olefin in ethylene oligomerization

Sen Lin [a], Lei Shi [b,*], Hongpeng Zhang [a], Na Zhang [b], Xianfeng Yi [c], Anmin Zheng [c], Xuebing Li [a,*]

[a] Qingdao Institute of Bioenergy and Bioprocess Technology, Chinese Academy of Sciences, No. 189 Songling Road, Laoshan District, Qingdao 266101, China
[b] Key Laboratory of Fine Chemicals in Universities of Shandong, Qilu University of Technology, Daxue Road, Changqing District, Jinan 250353, China
[c] Wuhan Institute of Physics and Mathematics, Chinese Academy of Sciences, West No. 30 Xiao Hong Shan, Wuhan 430071, China

ARTICLE INFO

Article history:
Received 23 July 2013
Received in revised form 10 October 2013
Accepted 11 October 2013
Available online 20 October 2013

Keywords:
Mesoporous materials
Plug-containing Al-SBA-15
Structural adjustment
Post-treatments
Ethylene oligomerization

ABSTRACT

Al-SBA-15 containing plug structures inside straight channels have been hydrothermally synthesized through a one-step synthesis strategy in an environmentally friendly acid-free medium. The effects of steaming, alkali, and acid post-treatments on the structural properties were investigated by powder X-ray diffraction (XRD), nitrogen adsorption–desorption at 77 K, transmission electron microscopy (TEM), scanning electron microscopy (SEM), FT-IR spectrum, ^{27}Al MAS NMR, and inductively coupled plasma (ICP) analyses. The presence of the plugs can significantly enhance structural stability against steaming or alkali post-treatments. Acid post-treatment can be a very simple and convenient technique for adjusting the textural properties of plug-containing Al-SBA-15, and especially for optimizing the accessibility to active sites. Acid post-treatment at the low temperatures of 313 and 323 K results in the formation of a larger specific surface area (905 m^2/g) and pore volume (0.94 cm^3/g) through an "open door" effect in the plugs, without eliminating any of the plugs from the channels. In particular, nearly half of the secondary micropores on the pore walls were preserved. In contrast, raising the acid post-treatment temperature further to 333 and 343 K caused a "closed doors" effect through the blockage of pores in the plugs by the extracted fragments. After loading with nickel, the catalyst exhibited a higher yield of C_{10+} olefins in ethylene oligomerization, and more importantly, after steaming and acid post-treatments at higher temperatures, the samples showed shape selectivity for the C_{16} olefin.

1. Introduction

Since the first report of M41S production by researchers at Mobil [1,2], ordered mesoporous molecular sieves have been the focus of numerous investigations dealing with their synthesis and exploring their potential as novel materials in a wide variety of research areas [3,4]. Indeed, their excellent structural properties, such as wide pore size, large surface area, large pore volume, and tunable composition make them versatile and suitable for a wide range of applications. However, their relatively low thermal and hydrothermal stabilities resulting from their amorphous nature still represent severe hurdles to their use for industrial applications. Therefore, research must aim at achieving stability while retaining and improving functionalization.

SBA-15 is one of the most important ordered mesoporous materials. It has two-dimensional (2-D) hexagonal *p6mm* symmetry and channel-type mesopores [5,6]. Because of its considerably thicker pore walls compared to MCM-41 [1,2], SBA-15 has better structural stability and has been regarded as one the most competitive candidates for use as a catalyst support for the conversion of bulk molecules. Many attempts have been made to prepare SBA-15-type mesoporous materials with large pore size, a goal that is of particular interest in order to accommodate molecules, especially those with very high molecular weight, such as enzymes [7,8].

Presently, high temperature synthesis (423–493 K) has been the most efficient and feasible method to synthesize mesoporous materials that have large pore size and that retain high hydrothermal stability. Vinu. et al. elaborated the synthesis of Al-SBA-15 with a pore size of ~12.5 nm at a temperature of 423 K [9,10]. Han et al. synthesized JLU-20 (pore size: >6 nm) at a reaction temperature of 433–493 K templated from a fluorocarbon–hydrocarbon surfactant mixture [11]. They believed that FC-4 prevents the ordering of the micelle matrix from collapsing thanks to its special stability at high temperatures. Inspired by this approach, another mesoporous material, JLU-21, with a three-dimensional (3D) cubic framework and a cage size of around 8 nm, was

* Corresponding authors. Tel./fax: +86 531 89631760 (L. Shi), tel.: +86 532 80662757; fax: +86 532 80662778 (X. Li).
E-mail addresses: leishi78@gmail.com (L. Shi), lixb@qibebt.ac.cn (X. Li).

1387-1811/$ - see front matter © 2013 Elsevier Inc. All rights reserved.
http://dx.doi.org/10.1016/j.micromeso.2013.10.016

synthesized at a temperature of 453 K [12]. Xiao et al. reported the synthesis of SBA-15 with a pore size of 10.5 nm using a single hydrocarbon surfactant (P123) as a structure-directing agent at 453 K [13]. Sang et al. prepared well-ordered mesoporous carbon by using SBA-15 as a hard template, which was synthesized at temperatures up to 513 K [14]. High temperature syntheses of other mesoporous silica materials, such as MCM-41 and JLU-30 have also been reported [15,16]. In addition, the microwave-assisted synthesis of ordered mesoporous silicas has gained popularity. Furthermore, the synthesis can be carried out at the high temperature of 473 K with the resulting material displaying a pore size of up to 11.4 nm [17].

Generally, the aforementioned mesoporous materials exhibit demonstrably enlarged pore diameter size with higher accessibility. More importantly, enhanced silica condensation was obtained at relatively higher reaction temperatures. Unfortunately, it is difficult to form a mesostructure with large specific surface area when the reaction temperature is higher than 423 K. On occasion, the resulting surface areas are even smaller than those of common microporous zeolites [11,13,14,16]. Striking a satisfactory balance between textural properties and hydrothermal stability hardly seems achievable using the high temperature synthesis strategy. Therefore, devising a simple and controllable method to synthesize SBA-15-type materials which possess excellent textural properties combined together with high framework stability still remains a challenge. Alternatively, the production of SBA-15-type mesoporous material with short pore-lengths has recently attracted much attention due to the better accessibility for molecules [18–26].

The synthesis of silicon-based mesoporous materials with excellent textural properties showing a novel pore structure with porous plugs inside the channels has been previously reported [27–33]. They exhibit uniform mesostructure, high stability, and are usually referred to as plugged hexagonal template silicas (PHTS). Their excellent thermal and hydrothermal stability are attributed to the existence of plugs inside the mesopores [28]. Characteristically, these materials principally exhibit a two-step desorption isotherm branch due to the presence of the blocked pores. It is noted that PHTS can be modified through the partial or complete dissolution of the aluminosilicate plugs. The specific structural properties of PHTS materials make it possible to combine the advantages of mesostructures and framework stability together.

It is well known that the large pores of mesoporous materials lead to a high diffusivity of large molecules rather than having suitability for shape selective applications. However, the selectivity for bulk molecules plays an important role in some catalytic conversions, especially concerning biomass conversion. Recently, there has been increasing interest in producing sulfur-free transportation fuels via low olefin oligomerization [34–36]. The critical point in this process is to maximize the concentration of hydrocarbons with a carbon chain longer than 10, since it directly affects the quality of the obtained transportation fuels. Considering the severe deactivation of zeolite-based catalysts, mainly due to the blocking of micropores with heavy products [37–39], mesostructure-based catalysts represent an interesting alternative [40]. However, only a negligible amount of C_{12+} product was obtained with the Ni/MCM-41 catalyst due to too high a product diffusion rate in the wide and straight mesopores [40].

In this paper, we report the direct synthesis of Al-SBA-15 with tunable aluminosilicate plug structures inside the straight mesopores in an acid-free medium. The high stability of this kind of mesoporous material is apparently due to the presence of plugs inside the straight channels that resist the steaming and alkali post-treatments. Furthermore, the blocked sections in the plug-containing Al-SBA-15 can be "opened" or "closed" through a controllable acid post-treatment. With this approach, the specific surface area, pore volume, and especially the accessibility of the pores, can be easily adjusted. After loading with Ni, the catalyst exhibited a high yield of C_{10+} olefin in ethylene oligomerization. More importantly, after being treated in acid conditions at temperatures of 333 and 343 K, the samples exhibited shape selectivity for the C_{16} linear olefin. We believe this work paves the way for adjusting the pore structure of mesoporous Al-SBA-15 to make it suitable for catalytic processes that require selectivity.

2. Materials

Al-SBA-15 was prepared using nonionic triblock copolymer pluronic P123 (Aldrich) as the structure-directing agent. Tetraethyl orthosilicate (TEOS, Sinopharm Chemical Reagent Co., Ltd) and aluminum nitrate 9-hydrate ($Al(NO_3)_3$ $9H_2O$, Aladdin Chemistry Co. Ltd) were used as silicon and aluminum sources, respectively. To optimize the pore structure of the obtained Al-SBA-15, 0.1 M oxalic acid (Sinopharm Chemical Reagent Co., Ltd) and sodium hydroxide (Aladdin Chemistry Co. Ltd) aqueous solutions were used in this work. All reagents were used as received.

2.1. Synthesis of plug-containing Al-SBA-15

The mesoporous Al-SBA-15 was synthesized according to the procedure we reported previously [41]. In a typical run, 1.0 g of the surfactant P123 was dissolved in 80 mL of water under magnetic stirring for a few hours at room temperature, after which 0.615 g of aluminum nitrate 9-hydrate was added into the gel and the mixture further stirred for 1 h. Then, 7.3 mL of TEOS was added to the clear solution and the mixture was kept under vigorous stirring for another 15 h at room temperature. Subsequently, the mixture was held at 313 K for 24 h under stirring and then it was transferred to an autoclave and heated at 363 K for 2 days under static conditions. The solid precipitate was recovered by filtration, washed several times with distilled water, and dried at 333 K overnight. To remove the surfactant by calcination, the solid was heated at a rate of 3 K min^{-1} up to 823 K, then held at this temperature for 5 h in air.

2.2. Steaming post-treatment

In a typical steaming post-treatment, 0.4 g of calcined plug-containing Al-SBA-15 was previously heated to 973 K at a heating rate of 3 K min^{-1} under an air flow of 100 mL/min. Then, the gas was changed to pure water vapor at the same temperature and maintained there for 4 h (referred to as HT-973 in this work).

2.3. Alkali post-treatment

Alkali post-treatment was performed in a 0.1 M sodium hydroxide aqueous solution. 700 mg of calcined sample was vigorously stirred in a 70 mL solution at various temperatures from 313 to 343 K for 0.5 h, referred to as BT-*x* in this work (*x*: treatment temperature). For example, BT-313 means that the plug-containing Al-SBA-15 was treated in a 0.1 M sodium hydroxide aqueous solution at 313 K for 0.5 h.

2.4. Acid post-treatment

The acid post-treatment procedure was carried out in a 0.1 M $H_2C_2O_4$ aqueous solution under the same conditions as that of the alkali post-treatment. Comparably, the prefix "AT" refers to acidic post-treatment and the treatment temperature is denoted by the suffix (referred to as AT-*x* in this work, *x*: treatment temperature).

2.5. Characterization

X-ray diffraction (XRD) measurements were carried out on a Bruker AXS-D8 Advance powder diffractometer, using Cu Kα radiation (40 kV, 40 mA), with a step size of 0.02° (2θ) and 2 s per step over the 2θ range from 0.5° to 8°. The nitrogen adsorption–desorption isotherms at 77 K were determined on an Autosorb®-6B instrument, using nitrogen of 99.999% purity. Prior to the experiments, the samples were outgassed for 6 h at 453 K, which was achieved using a heating rate of 1 K min^{-1}. The total specific surface area was calculated by the Brunauer–Emmett–Teller (BET) method, while the external specific surface area and the specific pore volume were obtained by the α_s method, using standard data for the adsorption of nitrogen on non-porous, partially hydroxylated silica to construct the α_s plots. The pore volume of the blocked mesopores was calculated from the second desorption step, ranging from the second inflection point to the closing point of the hysteresis loop. Mesopore diameters were obtained from the maximum pore size distribution (PSD) calculated from the adsorption branch by the non-local density functional theory (NLDFT) method, using QuadraWin™ software from Quantachrome. Scanning electron microscopy (SEM) was performed on a Hitachi H-4800 microscope. Transmission electron microscopy (TEM) studies were carried out on a Hitachi H-7650 electron microscope with an accelerating voltage of 100 kV. The chemical composition of the resulting material was determined by an Optima 2000DV, Inductive Coupled Plasma Emission Spectrometer (ICP). All ^{27}Al NMR experiments were performed on a Bruker Ascend-500 spectrometer at a resonance frequency of 130.44 MHz with a 4 mm triple-resonance MAS probe at a sample spinning rate of 10 kHz. The pulse width (π/2) for ^{27}Al was measured to be 1.5 μs. ^{27}Al MAS NMR spectra were recorded using a small-flip-angle technique with a pulse length of 0.25 μs (π/12) and a recycle delay of 1 s. The chemical shift of ^{27}Al was externally referenced to 1 M aqueous Al $(NO_3)_3$. Temperature-programmed desorption of ammonia (NH_3-TPD) for acidity analysis was carried out in a Micromeritics Autochem–Chemisorption Analyzer. 150 mg of the sample was pretreated at 873 K in Ar flow for 2 h. After cooled down to room temperature (around 298 K in this work), a pure NH_3 was adsorbed for 2 h. Desorption of NH_3 was monitored in the temperature range of 373–773 K with the heating rate of 10 K/min.

2.6. Catalytic experiment

The catalytic experiment was performed in a fixed-bed microreactor. The catalysts were prepared by impregnation of required Al-SBA-15 with 0.1 M $Ni(NO_3)_2$ aqueous solution, followed by calcination in air at 723 K for 2 h. Then, the catalyst powder was first formed under pressure, and then crushed into pellets with a mean particle size in the range of 60–80 mesh. Prior to each experiment, the catalysts were pretreated in a tubular electric furnace (723 K, 2 h) under H_2–N_2 flow (H_2/N_2 = 3:7) at atmospheric pressure. Then, the catalyst pellets (Ni loading amount: 5%, 60–80 mesh) were mixed with an equal amount of quartz sand and transferred to the reactor. The reactor was then heated to 393 K under He flow (20 mL/min). Then, the conversion of ethylene was carried out under the experimental pressure (3.0 MPa in this work). On- and off-line analyses for gas and liquid products were carried out using Agilent 7890 gas chromatographs equipped with Plot-Q and BP-1 capillary columns, respectively. The compositions of liquid products were identified using 5975 inert XL MSD GC/MS instrument (Agilent).

3. Results and discussion

Fig. 1A shows that the resulting plug-containing Al-SBA-15 has three distinct diffraction peaks at 2θ = 0.88°, 1.50°, and 1.73°, indexed to the (100), (110), and (200) planes, respectively, in the 2D hexagonal *p6mm* symmetry, indicating that well-ordered Al-SBA-15 was obtained. The wheat-like aggregated morphology consisting of long rod-like particles can be seen in Fig. 2A. The mean diameter and length of the rod-like particles are 600–800 nm and several micrometers, respectively, similar to that of Al-SBA-15 synthesized in the conventional strong acidic medium [5,6]. The clear and gray stripes seen in the transmission electron microscope (TEM) image (Fig. 2B) taken along (110) correspond to parallel cylindrical channels and wall structures, respectively. The bright

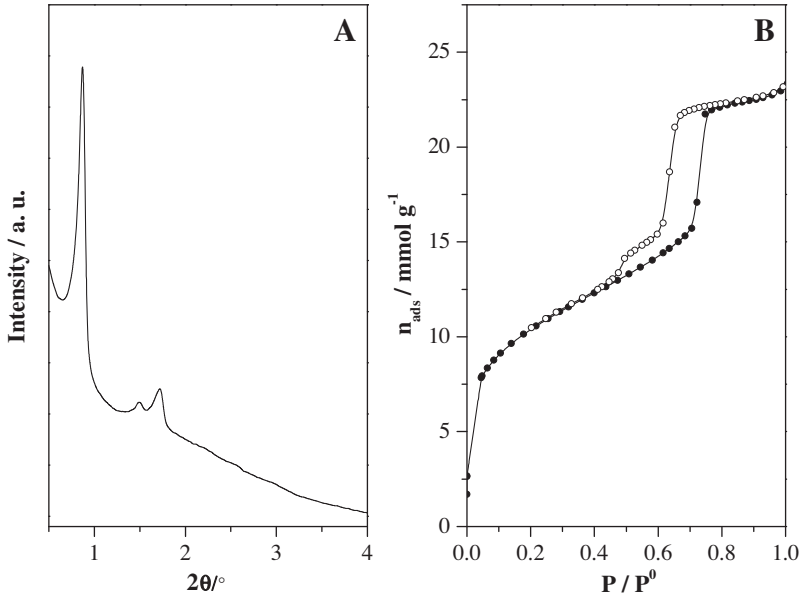

Fig. 1. (A) Small-angle X-ray diffraction pattern and (B) nitrogen adsorption–desorption isotherm at 77 K (closed symbols-adsorption) determined on calcined Al-SBA-15 synthesized, without addition of mineral acid, at 363 K with a P123/Si molar ratio of 0.0050.

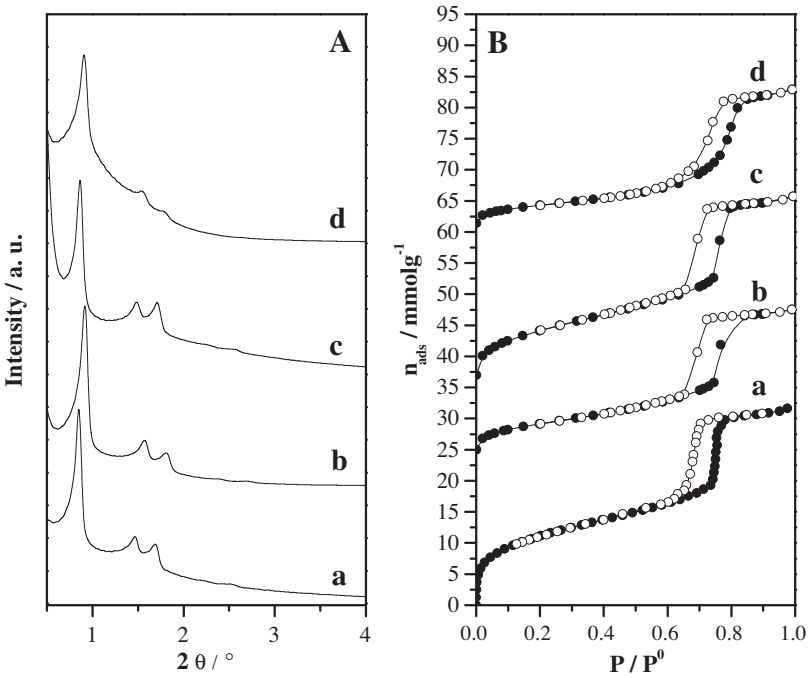

Fig. 2. (A) Small-angle X-ray diffraction pattern and (B) nitrogen adsorption–desorption isotherm at 77 K (closed symbols-adsorption) determined on (a) Al-SBA-15 without plugs, (b) Al-SBA-15 without plugs after steaming treatment, (c) Al-SBA-15 without plugs after acid treatment, and (d) Al-SBA-15 without plugs after basic treatment.

Table 1
Influence of steaming (Prefix: HT), basic (Prefix: BT), and acidic (Prefix: AT) post-treatments on structural properties of plug-containing Al-SBA-15 synthesized in acid-free system at 363 K determined from ICP, N_2 sorption, and XRD data.

Sample	T(K)	Si/Al	a_0 (nm)	A_{BET} ($m^2\ g^{-1}$)	A_{ext} ($m^2\ g^{-1}$)	V_p ($cm^3\ g^{-1}$)	V_{mic} ($cm^3\ g^{-1}$)	V_{mes} ($cm^3\ g^{-1}$)	$V_{mes,\ blocked}$($cm^3\ g^{-1}$)	$V_{mes,\ blocked}$(%)	D_p (nm)	t (nm)
Al-SBA-15	—	30.4	12.0	841	31	0.74	0.08	0.66	0.14	21.2	7.3	4.4
HT-973	973	46.1	10.8	416	21	0.48	0.02	0.46	0.14	30.0	7.0	3.8
BT-313	313	28.0	11.9	502	34	0.66	0.01	0.65	0.10	15.4	7.3	4.3
BT-323	323	28.5	12.0	528	43	0.73	0	0.73	0.10	13.7	7.6	4.4
BT-333	333	27.7	11.9	518	47	0.73	0.01	0.72	0	0	7.6	4.3
BT-343	343	25.3	11.7	505	53	0.72	0.01	0.71	0	0	7.9	3.8
AT-313	313	38.3	12.0	862	36	0.81	0.08	0.73	0.07	9.6	7.3	4.7
AT-323	323	39.8	12.0	905	45	0.94	0.06	0.88	0.04	4.5	7.6	4.4
AT-333	333	38.5	12.1	760	31	0.63	0.04	0.59	0.21	35.6	7.3	4.8
AT-343	343	42.1	12.1	770	33	0.64	0.04	0.60	0.18	30.0	7.3	4.8

a_0 – unit cell parameter determined by XRD. A_{BET} – total specific surface area obtained by BET method. A_{ext}, V_p, and V_{mic} – external specific surface area, total pore volume, and micropore volume, in terms of equivalent liquid volume, obtained by α_s method. V_{mes} – mesopore volume, caculated as $V_{meso} = V_{total} - V_{micro}$. $V_{mes,blocked}$ – volume of blocked mesopores. $V_{mes,\ blocked}$ (%) – percentage of blocked mesopores to total mesopores. D_p – mesopore diameter corresponding to maximum of the PSD calculated by NLDFT method from adsorption branch; t – wall thickness, calculated as $t = a_0 - D_p$.

spots visible within the striped pattern are due to cavities in the mesopores.

Nitrogen sorption isotherms for plug-containing Al-SBA-15 as shown in Fig. 1B are of type IV in the IUPAC classification scheme, with a sharp capillary condensation step indicative of a narrow pore size distribution. The pore size diameter was calculated to be 7.3 nm (SI Fig. 1A). The hysteresis loop appears in the P/P^0 range of 0.46–0.76. The desorption branch of the hysteresis loop is composed of two parts: the first ranging from 0.76 to 0.60 P/P^0 corresponds to open straight mesopores, while the second from 0.60 to 0.46 P/P^0 corresponds to blocked mesopores, as reported previously [27–29,31,32,41]. This result demonstrates the presence of plug structures inside the mesopores. The blocked sections were calculated to be 21.2% of the total mesopore volume (Table 1). The pronounced increase of N_2 adsorption detected in the 0.10–0.70 P/P^0 range is characteristic of porosity in the plugs, as shown by Van Der Voort et al. [28]. Herein, the adsorption in the same relative pressure range can be explained by multilayer adsorption of N_2 molecules.

The acid-free synthesis is a simple and environmentally-friendly method for the formation of Al-SBA-15 with high structural stability [41]. As shown in Fig. 2, Al-SBA-15 without plugs after steaming, acid and basic post-treatments showed three well-resolved XRD diffraction peaks, indicating that structural ordering was generally maintained. Notably, the formation of the plugs in mesoporous Al-SBA-15 can improve its structural stability. The plug-containing Al-SBA-15 after steaming treatment has a micropore volume of 0.02 cm^3/g, while non-micropore volume was detected for the Al-SBA-15 without plugs. This result suggests that all the secondary pores on the walls of Al-SBA-15 without plugs were destroyed during post-treatment. Additionally, after basic treatment, plug-containing Al-SBA-15 showed a significant reduction of BET surface

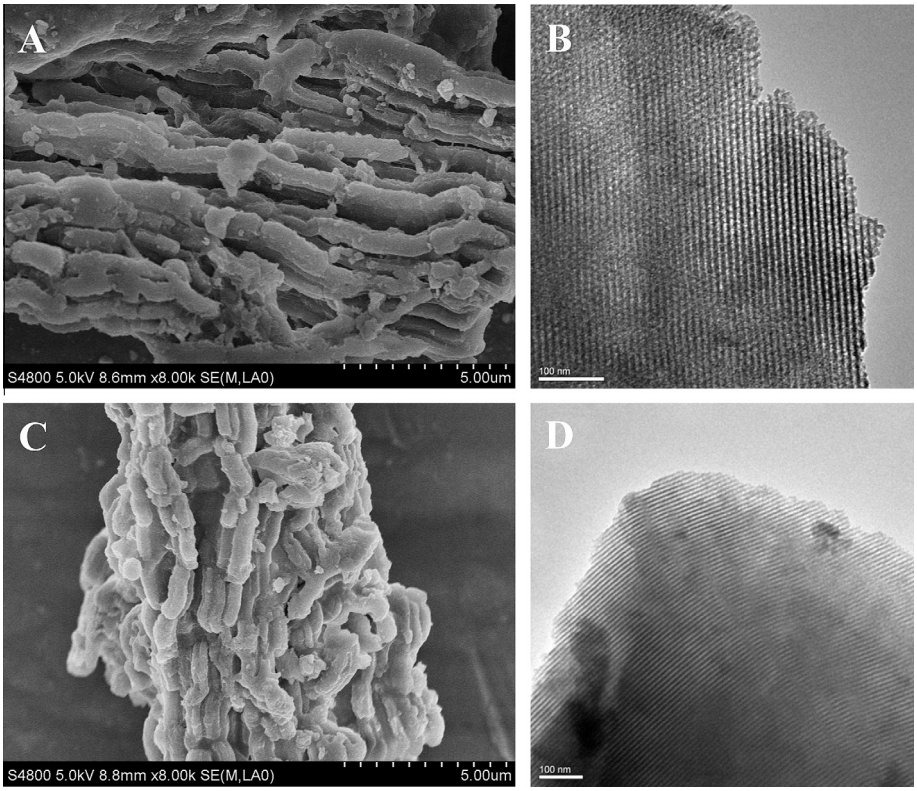

Fig. 3. (A) SEM image and (B) typical TEM image of calcined Al-SBA-15, synthesized with P123/Si molar ratio of 0.0050 in initial acid-free reaction solution. (C) SEM image and (D) typical TEM image of Al-SBA-15 after steaming post-treatment.

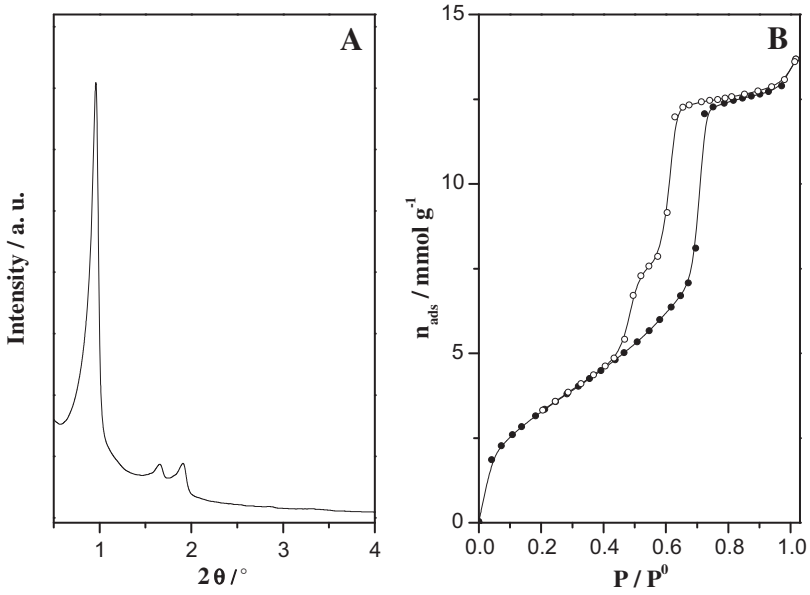

Fig. 4. (A) Small-angle X-ray diffraction pattern and (B) nitrogen adsorption–desorption isotherm at 77 K (closed symbols-adsorption) determined on calcined Al-SBA-15 after steaming post-treatment.

area of around 40% (from 841 to 505 m^2/g). Comparably, the proportion was calculated to be as high as 63% (from 935 to 343 m^2/g) for the Al-SBA-15 without plugs, as shown in SI Table 1. These results confirm that the presence of plugs can obviously enhance the structural stability of Al-SBA-15 against severe post-treatment.

It is concluded that the structural stability of PHTS materials benefits from plugs inside the mesopores, which act as supporting structures to suppress the collapse of the framework under severe treatement conditions [28]. The stability and properties of plug-containing Al-SBA-15 under steaming were characterized with XRD, N_2-sorption, SEM, TEM (Figs. 3, 4, and Table 1). The plug-containing Al-SBA-15 exhibited high structural stability after the steaming post-treatment (Fig. 4A). The treated sample displays a similar morphology and ordered mesostructure to non-treated samples (Fig. 3C, D). However, marked reductions in the specific

surface area and pore volume were observed, calculated as 51% (from 841 to 416 m^2/g) and 35% (from 0.74 to 0.48 cm^3/g), respectively, indicating the partial collapse of the mesostructure, despite the presence of plugs inside the mesopores. In addition, the treated sample exhibits a lower adsorption volume at a low relative pressure (0–0.1 P/P^0), due to the lack of microporosity. Further study of the isotherms showed that the adsorption in 0.1–0.6 P/P^0 for the treated sample is lower than that of non-treated Al-SBA-15, due to the lack of super micropores. A two-step desorption branch appeared, indicative of the pore plugging effect. Steaming also had an effect on the chemical composition of the material. Al-SBA-15 showed a higher Si/Al molar ratio, rising from 30.4 to 46.1, indicative of a de-aluminization process during the steaming post-treatment.

The alkali post-treatment technique can extract framework silicon from microporous zeolite through the selective activation of the Si—O—Si bond [42,43]. We therefore studied the effect of plug structure on the stability of SBA-15-type mesoporous materials in alkali conditions. Noticeably, Al-SBA-15 without plugs synthesized from a conventional strong acidic medium lost most of its ordered mesostructure (SI Fig. 2) after an alkali post-treatment. When varying the temperature from 273 to 333 K, the samples all exhibited blurry (100) peaks and simultaneously, the (110) and (200) peaks disappeared, indicative of the severe collapse of the mesostructure [42–45].

Because of the relatively lower aluminum concentration in plug-containing Al-SBA-15 (Si/Al = 30.4) than in the aforementioned Al-SBA-15 without plugs (Si/Al = 22.0), the Si—O—Si bond in the former should be more sensitive to the basic treatment [46]. However, the structural ordering of plug-containing Al-SBA-15 was efficiently preserved after alkali post-treatment, even at a temperature of 343 K; this result is supported by the observation of three well-resolved peaks in the XRD results as viewed in Fig. 5A. Furthermore, the alkali treated sample exhibits a stronger (110) diffraction peak compared to the original sample. The calculated intensity ratio Int.(110)/Int.(200) increased from around 0.4 to 1.2 (Figs. 1A, 5A), and is surprising because the treated sample would be expected to have thinner walls, as suggested for the hexagonal mesostructure of MCM-41 [47,41]. However, the wall

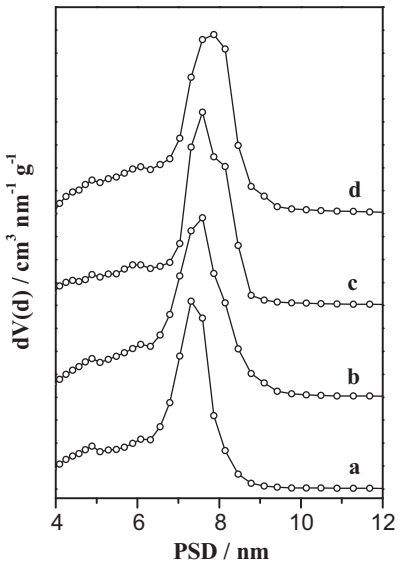

Fig. 6. NLDFT pore size distribution curves calculated from adsorption branches of (a) BT-313, (b) BT-323, (c) BT-333, and (d) BT-343.

thickness of alkali treated Al-SBA-15 was calculated to be around 4.3 nm at treatment temperatures below 343 K, very close to that of the initial sample (4.4 nm). The morphology and particle size (SI Fig. 3) were barely affected by the basic treatment. Therefore, we suggest that the intense (110) peak can be ascribed to the formation of higher structural ordering along the (110) direction [48], resulting from the elimination of the plugs under alkali conditions.

Fig. 5B and Fig. 6 depicts the effect of post-treatment temperature on the porosity of plug-containing Al-SBA-15 under alkali conditions. (Fig. 6). Obviously, evaporation in the desorption branch corresponding to the blocked mesopores was found to decline at higher temperatures. We propose that the elimination of the plugs leads to the formation of open-form mesopores. The blocked sections were found to have completely disappeared for BT-333,

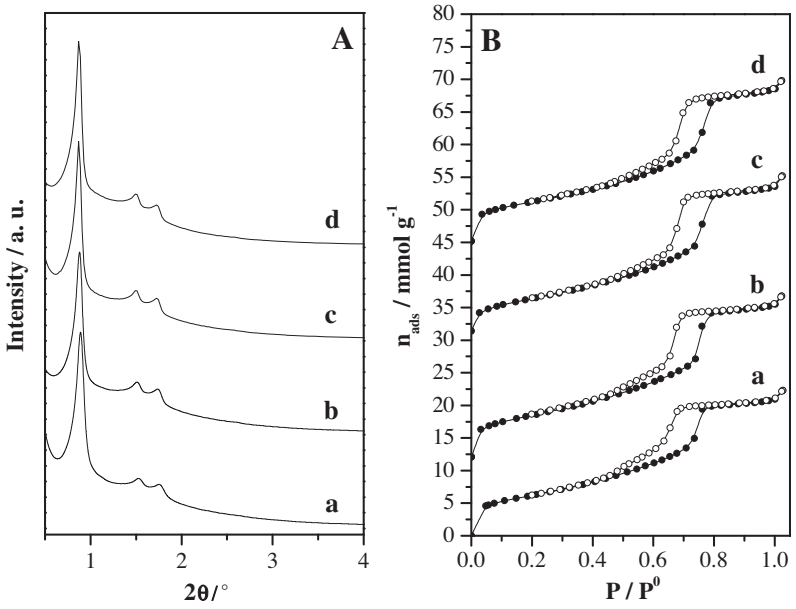

Fig. 5. (A) Powder X-ray diffraction patterns and (B) nitrogen adsorption–desorption isotherms at 77 K (closed symbols-adsorption) determined on (a) BT-313, (b) BT-323, (c) BT-333, and (d) BT-343. The isotherms were offset vertically by 14, 32, and 45 mmol g^{-1}, respectively.

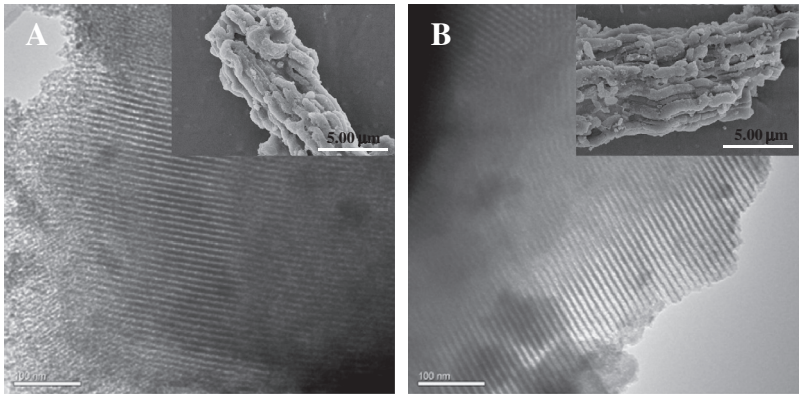

Fig. 7. TEM and SEM images (insert) of (A) BT-323 and (B) AT-323.

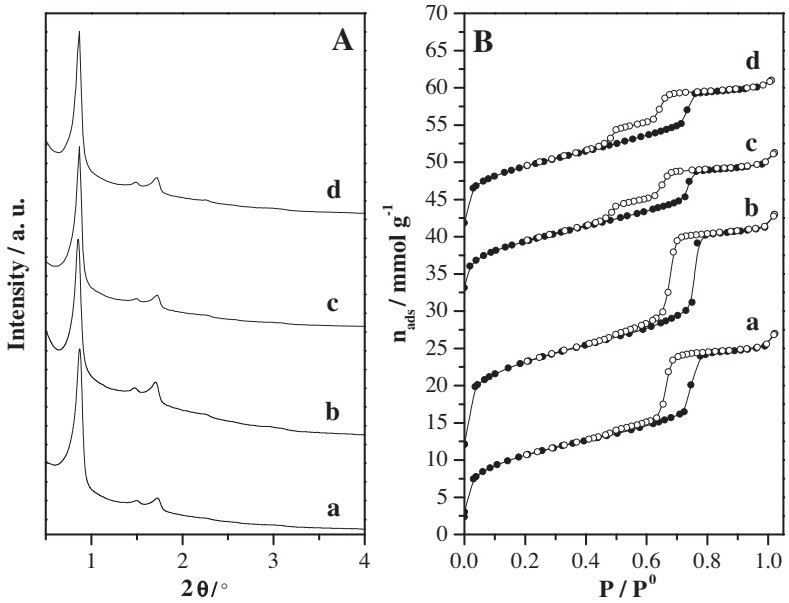

Fig. 8. (A) Powder X-ray diffraction patterns and (B) nitrogen adsorption–desorption isotherms at 77 K (closed symbols-adsorption) determined on (a) AT-313, (b) AT-323, (c) AT-333, and (d) AT-343. The isotherms were offset vertically by 10, 30, and 40 mmol g^{-1}, respectively.

meaning a very open and uniform mesostructure was formed, in agreement with the XRD results. On the other hand, a higher contrast between the stripes assigned to wall and channels was found for Al-SBA-15 after alkali post-treatment (Fig. 7A). This result further confirms that the structural ordering of the plug-containing Al-SBA-15 was effectively preserved during the alkali post-treatment. This is in contrast with the measurement of a reduced specific surface area of 505 m^2/g after alkali post-treatment, a possible sign that the ordering of the structure might have partially collapsed due to the activation of Si—O—Si bonds (Table 1) under basic conditions. Nevertheless, the alkali-treated samples exhibited considerable pore volume, almost equal to those found with prior treatments. In addition, after alkali treatment the samples have a lower Si/Al molar ratio due to the selective activation of the Si—O—Si bond under basic conditions [44]. It has been reported that the condensation mechanisms of the wall structure and plugs are different [28,49]. Yet, considering the amorphous nature of SBA-15-type mesoporous materials, we propose that silicon extraction takes place homogeneously on the exposed surface to form a wider pore size distribution as shown in Fig. 5. We therefore suggest that alkali post-treatment can deeply influence the structural properties of plug-containing Al-SBA-15 through the dissolution of plugs and pore walls. The presence of plugs can increase the structural stability of Al-SBA-15 under the alkali treatment by weakening the interaction between alkali molecules and the internal surface. We therefore confirm that the high stability of the structural ordering in plug-containing Al-SBA-15 is mainly related to the presence of plugs.

The various effects of acidic post-treatment on the structure of plug-containing Al-SBA-15 are shown in Figs. 7–9, and Table 1. Al-SBA-15 containing plugs exhibits very high stability in the acidic medium. All acid-treated samples gave XRD diffraction patterns and cell sizes similar to those previously treated (Fig. 8A and Table 1). The hexagonal mesostructrue and morphology (Fig. 7 and SI Fig. 4) were also preserved. It is well known that acid post-treatment tends to selectively remove aluminum from the framework to modify the acidic properties and pore structure in zeolites [50–52]. The ICP results indicate that all of the acid-treated samples have a higher Si/Al ratio than initially due to the removal of aluminum from the Al-SBA-15 framework, independent of the treatment temperature. Meanwhile, aluminum leaching did not affect either the ordering of the mesostructure or the cell

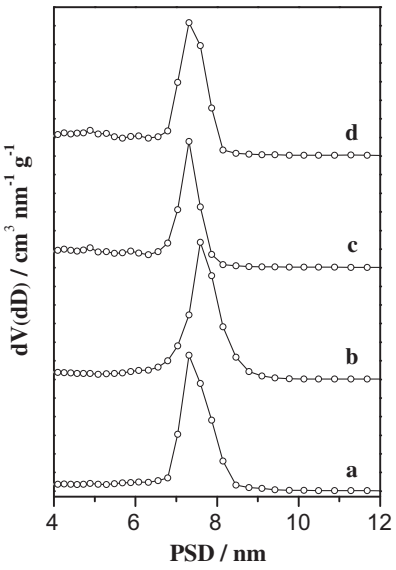

Fig. 9. NLDFT pore size distribution curves calculated from adsorption branches of (a) AT-313, (b) AT-323, (c) AT-333, and (d) AT-343.

parameters. All samples which underwent acid post-treatment exhibit a weak (110) diffraction peak, the same as prior to treatment. As already discussed above, the weak (110) diffraction peak observed here is attributed to the presence of plug structures inside channels rather than to the formation of poorer ordering along this direction. In this case, it is proposed that the plugs are still located inside the mesopores of the acid-treated samples, a conclusion that is also supported by the observation of Al-SBA-15 particles with a sharper external surface than that of the alkali-treated samples (Fig. 7 and SI Fig. 4).

Nitrogen sorption isotherms for the acid-treated Al-SBA-15 samples are shown in Fig. 8B and the textural properties summarized in Table 1. All samples display type IV isotherms with a sharp capillary condensation, along with an H1-type hysteresis loop, similar to that of pure Al-SBA-15. When samples were treated at 313 and 323 K under acidic conditions, the desorption branches exhibited an indistinct two-step capillary evaporation. In contrast, by increasing the treatment temperature to 333 and 343 K, a clear two-step desorption branch can be observed. Considering the presence of plugs inside the mesopores of these samples, the apparent difference in the shape of the desorption branches is attributed to the various pore structures within the plugs.

AT-323 showed a pore size of 7.6 nm, slightly wider than that of plug-containing Al-SBA-15 (7.3 nm), and indicating that the framework aluminum had been extracted from the internal surfaces of the mesopores [53]. AT-313 and AT-323 have specific surface areas of 862 and 905 m^2/g, respectively, a value which is slightly greater than that prior to treatment (841 m^2/g). The pore volumes were calculated as 0.81 and 0.94 cm^3/g, greater than that of the initial sample (0.74 cm^3/g). For materials with similar characteristics, Bavel et al. have reported that the channels behind the plugs are inaccessible for hydrocarbons such as *n*-hexane [54]. Therefore, the large AT-323 pore volume of 0.91 cm^3/g, being 23% higher than that of the initial value (0.74 cm^3/g), may be due to more adsorption in the blocked sections. In other words, acidic post-treatment at relatively lower temperature favors the "open door" mechanism at the plugs, allowing N_2 to enter previously inaccessible sections. In addition, treatment in an acidic medium at low temperatures (313 and 323 K) maintains the micropore structure, which is evidenced by a micropore volume of 0.08 and 0.06 cm^3/g for AT-313 and AT-323, respectively. These values are slightly lower than that of the samples prior to treatment (0.08 cm^3/g), which can be 2attributed to the leaching of aluminum from pore walls and plugs. The adsorption behavior in the relative pressure range of 0.1–0.7 P/P^0 revealed that AT-333 and AT-343 have similar multilayer N_2 adsorptions compared to those of AT-313 and AT-323, resulting from the presence of porous plugs inside the channel. However, the distinctive two-step desorption branches, smaller pore volumes and specific surface areas confirm the formation of new inaccessible sections inside the channels. The fraction of blocked mesopores to total mesopores was calculated as 35.6% and 30.0% for AT-333 and AT-343, respectively, values which are higher than that of the samples prior to treatment (21.2%). We suggest that the fragments leached from the pore walls and the plugs can block the pores of nearby plugs to form denser plugs which are more difficult to erode under the acid conditions used in this work. This would also account for the slightly higher Si/Al molar ratio of 38.5 and 42.1 for AT-333 and AT-343, respectively. Apparently, the formation of denser plugs hinders the etching effect and protects the framework. Therefore, the "door" on the plugs can be physically closed in the acid post-treatment at a relatively higher temperature.

3.1. Catalytic test

Table 2 summarizes the catalytic performance of the various samples for ethylene oligomerization, especially the distribution of product under a mild reaction temperature and high pressure. Clearly, Ni-loaded PHTS-type Al-SBA-15 is an active catalyst in ethylene oligomerization that is produced by the mesostructure and appropriate acidity [40,55]. The presentation of around a 30% yield of C_{10+} olefins in the liquid product is due to the highly accessible channels (SI Fig. 5) [56]. This result also insures that the pores on the plug structures are large enough to assure a high diffusion of reactant and by-product molecules during ethylene oligomerization. Ni/BT-333 has more open pores than the others since the plugs have been dissolved away during alkali post-treatment, a property that also plays an important role in inducing the absence of C_{16} linear olefin in the liquid product. Although trace amounts of C_{16} linear olefin can be detected in the liquid product by using Ni/AT-323 as catalyst, the effect of structural adjustment on the product distribution is still very weak. On the other hand, C_{16} linear olefin amounts of 2.1% and 1.4% in the liquid product were detected for Ni/HT-973 and Ni/AT-343, respectively.

As for HT-973, the higher selectivity to C_{16} linear olefin is due to the blocking of channels resulting from the significant collapse of the ordered mesostructure during hydrothermal post-treatment (Fig. 10B). It is well known that the ethylene oligomerization is strongly dependent on the acidity of the catalyst, which directly related to the nature of support. Considering that the Ni/HT-973 showed the highest selectivity for C_{16} linear olefin in ethylene oligomerization among all prepared catalysts, the acidic properties of plug-containing Al-SBA-15 and HT-973 were investigated by

Table 2
Ethylene oligomerization over Ni-loading catalysts[a].

Catalyst	Con. of ethylene(%)[b]	Sel. of C_{10+} (%)	Sel. of C_{16} linear olefin (%)
Ni/Al-SBA-15	100	29.8	–
Ni/HT-973	95	34.7	2.1
Ni/BT-333	100	28.4	–
Ni/AT-323	75	31.2	trace
Ni/AT-343	91	35.1	1.4

[a] Catalyst charge = 1.0 g (60–80 mesh); reaction pressure = 3.0 MPa; ethylene feed rate = 13.6 mL/min.
[b] Duration of reaction = 6 h.

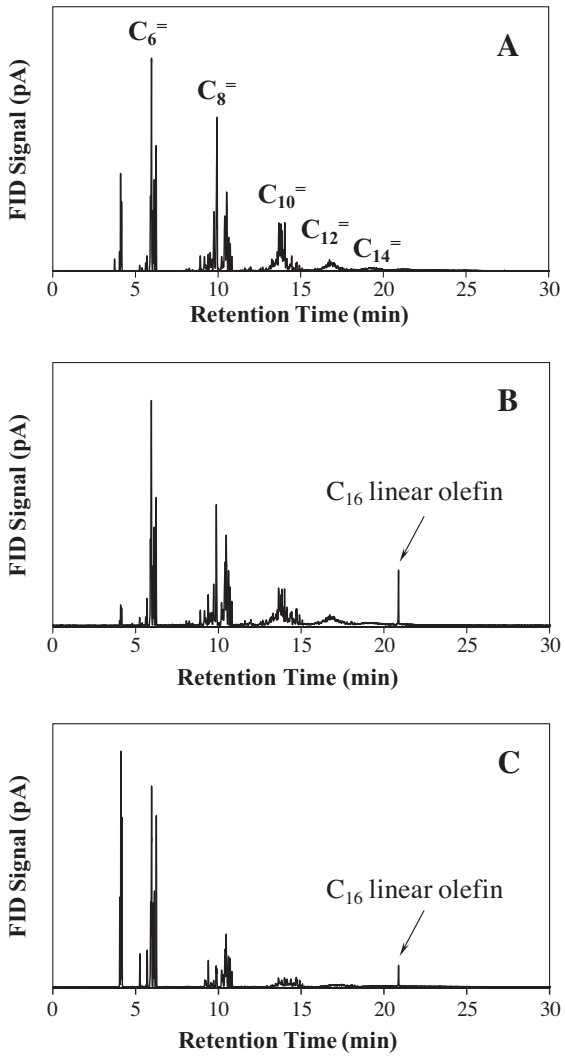

Fig. 10. Composition of liquid production derived from ethylene oligomerization over (A) Ni/plug-containing Al-SBA-15, (B) Ni/HT-973, and (C) Ni/AT-343.

NH_3-TPD, and the results are shown in Fig. 11. HT-973 exhibits the similar acidic strength and distribution to that of the plug-containing Al-SBA-15, consisting of two peaks centered at 460 and 570 K, which is associated with the weak acidity resulting from the amorphous nature. This suggested that the interaction between nickel precursor and support (HT-973) is similar to that on Ni-Al-SBA-15 catalyst. Therefore, it is concluded that the high selectivity of 2.1% for C_{16} linear olefin over Ni/HT-973 ascribes to its structural property.

In contrast, although some large pores were formed in the walls and plugs of AT-343, the pores on the plugs were physically blocked by fragments during the acid post-treatment, which created more blocked sections in the straight mesopores. So, the relatively lower diffusivity of the intermediates in these blocked sections accelerates the formation of long chain hydrocarbons (Fig. 10C). The selective leaching of Al and Si occurred during the acid and basic treatments, which changed the properties of the Al species, such as coordination state, content, and distribution, accordingly leading to the formation of various acidic properties of the support. The interaction between the nickel precursor and the acid sites on Al-SBA-15 after acid and basic treatments are different than those of Ni/Al-SBA-15 and Ni/HT-973. The nickel species therefore have shown various properties after calcination, such as composition, particle size, dispersion etc., for Ni/AT and Ni/BT, which also apparently influence the catalytic pathway [35,57,58]. Although Ni/AT-343 exhibited a surprising C_{16} linear olefin selectivity of 1.4% in the liquid product and the pores in the plugs were "closed" during the post-treatment, the systematic investigation focused on the Ni-acid site interaction and they still need to be carried out to better understand the catalytic properties. These results will be discussed separately in the near future.

Fig. 12 gives the ^{27}Al MAS NMR spectra of selected samples. The plug-containing Al-SBA-15 shows two peaks centered at around 52 ppm and −0.8 ppm (Fig. 12a). The former resonance is attributed to Al in tetrahedral coordination (AlO_4 structural unit, Al(tet)), while the latter peaks are assigned to two types of sixfold-coordinated Al (AlO_6 structural unit, Al(oct)), respectively. Despite the post-treatments (steaming, basic, or acidic), the resulting samples exhibit only one peak assigned to the AlO_4 structural unit, demonstrating that the aluminum is located mainly at tetrahedrally coordinated sites to produce Brønsted acid sites through Si—O—Al

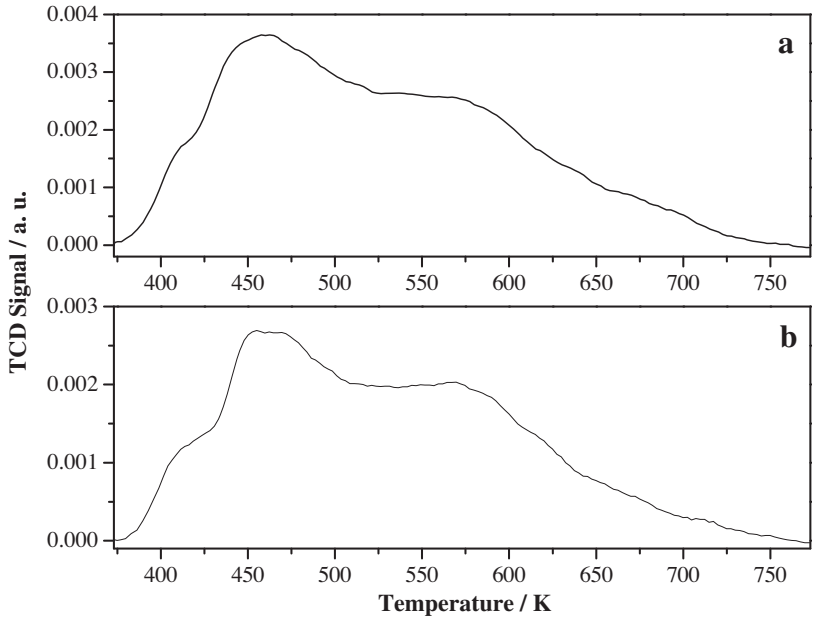

Fig. 11. NH_3-TPD patterns of (a) plug-containing Al-SBA-15 and (b) HT-973.

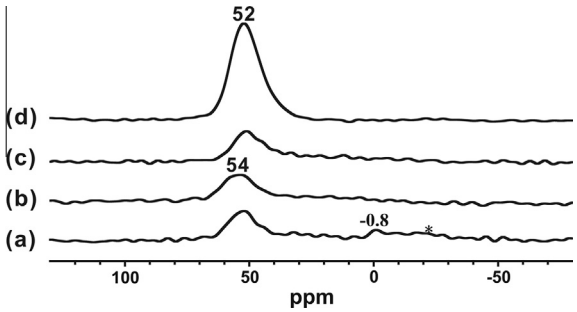

Fig. 12. ^{27}Al MAS NMR spectra of (a) plug-containing Al-SBA-15, (b) HT-973, (c) AT-343, and (d) BT-333.

linkage, which is responsible for an ethylene conversion of greater than 91% (Table 2). The absence of an octahedrally coordinated aluminum signal for the samples after post-treatment is due to the dissolution of non-framework aluminum. BT-333 has the best aluminum coordination environment compared to the others, a conclusion that is supported by the observation of a sharp peak at 52 ppm (Fig. 12d). However, it exhibits a C_{10+} selectivity of 28.4%, which is apparently lower than that of the samples after steaming and acid post-treatments, as evidenced by the fact that the distribution of products from ethylene oligomerization can be readily adjusted by tuning the pore structure.

4. Conclusion

Al-SBA-15 containing plugs inside mesopores was directly synthesized in a synthetic medium without any additional mineral acid. The comprehensive results confirm that the presence of plugs can remarkably enhance the structural stability of SBA-15-type mesoporous material in withstanding steaming, alkali, and acid post-treatments. The pore structure can be simply and efficiently adjusted.

(i) Steaming post-treatment leads to lower structural ordering and the formation of large pores in the pore wall, besides the elimination of plugs (Fig. 13A).
(ii) Alkali post-treatment results in the collapse of the ordered mesostructure through selective activation of the Si—O—Si bond, and simultaneously, the secondary pores on the wall were enlarged. Its effect on the structure was identified as the dissolution of plugs and pore wall structure (Fig. 13B).
(iii) Acidic post-treatment at a relatively lower temperature can be regarded as an approximate "open door" effect in the plugs. This effect can remarkably increase the specific surface area and pore volume, and then an ordered mesoporous material with high structural stability and textural properties, as well as high accessibility, is obtained (Fig. 13C).
(iv) By increasing the acidic post-treatment temperature to 333 and 343 K, most of the pores in the plugs are blocked by the accumulation of fragments extracted from the pore walls and plugs. This result demonstrates that the shape-selectivity effect can be achieved on mesoporous materials (Fig. 13D).

Acknowledgments

This work was supported by a grant from National Natural Science Foundation of China (51202134) and 100-Talent Project of Chinese Academy of Science Foundation (Grant KJCX2-EW-H05). The authors sincerely thank Dr. Charlotte Bonneau, Prof. Robert I Boughton and Miss. Yan Xu for the valuable discussions. This work partially supported by a grant from Shangdong Province Young and Middle-Aged Scientists Research Awards Fund (BS2012CL027).

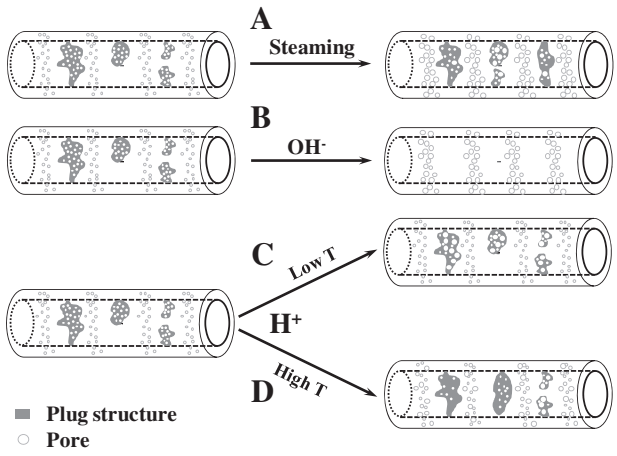

Fig. 13. Schematic representation of structural tuning process of plug-containing Al-SBA-15 during (A) steaming, (B) alkali, and (C), (D) acidic post-treatment at relatively low and high temperature, respectively.

Appendix A. Supplementary data

Supplementary data associated with this article can be found, in the online version, at http://dx.doi.org/10.1016/j.micromeso.2013.10.016.

References

[1] C.T. Kresge, M.E. Leonowicz, W.J. Roth, J.C. Vartuli, J.S. Beck, Nature 359 (1992) 710–712.
[2] J.S. Beck, J.C. Vartuli, W.J. Roth, M.E. Leonowicz, C.T. Kresge, K.D. Schmitt, C.T.-W. Chu, D.H. Olson, E.W. Sheppard, S.B. McCullen, J.B. Higgins, J.L. Schlenker, J. Am. Chem. Soc. 114 (1992) 10834–10843.
[3] A. Taguchi, F. Schüth, Microporous Mesoporous Mater. 77 (2005) 1–96.
[4] A. Corma, Chem. Rev. 97 (1997) 2373–2419.
[5] D. Zhao, J. Feng, Q. Huo, N. Melosh, G.H. Fredickson, B.F. Chmelka, G.D. Stucky, Science 279 (1998) 548–552.
[6] D. Zhao, Q. Huo, J. Feng, B.F. Chmelka, G.D. Stucky, J. Am. Chem. Soc. 120 (1998) 6024–6036.
[7] J. Liu, C. Li, Q. Yang, J. Yang, C. Li, Langmuir 23 (2007) 7255–7262.
[8] Z. Zhou, M. Hartmann, Chem. Soc. Rev. 42 (2013) 3894–3912.
[9] A. Vinu, V. Murugesan, W. Böhlmann, M. Hartmann, J. Phys. Chem. B 108 (2004) 11496–11505.
[10] M. Hartmann, A. Vinu, Langmuir 18 (2002) 8010–8016.
[11] Y. Han, D. Li, L. Zhao, J. Song, X. Yang, N. Li, Y. Di, C. Li, S. Wu, X. Xu, X. Meng, K. Lin, F.-S. Xiao, Angew. Chem. Int. Ed. 42 (2003) 3633–3637.
[12] D. Li, Y. Han, J. Song, L. Zhao, X. Xu, Y. Di, F.-S. Xiao, Chem. Eur. J. 10 (2004) 5911–5922.
[13] N. Xiao, L. Wang, S. Liu, Y. Zou, C. Wang, Y. Ji, J. Song, F. Li, X. Meng, F.-S. Xiao, J. Mater. Chem. 19 (2009) 661–665.
[14] L.-C. Sang, A. Vinu, M.-O. Coppens, J. Mater. Chem. 21 (2011) 7410–7417.
[15] K. Zhang, H.-L. Chen, B. Albela, J.-G. Jiang, Y.-M. Wang, M.-Y. He, L. Bonneviot, Eur. J. Inorg. Chem. 3 (2011) 59–67.
[16] X. Yang, S. Zhang, Z. Qiu, G. Tian, Y. Feng, F.-S. Xiao, J. Phys. Chem. B 108 (2004) 4696–4700.
[17] E.B. Celer, M. Jaroniec, J. Am. Chem. Soc. 128 (2006) 14408–14414.
[18] K. Kosuge, T. Sato, N. Kikukawa, M. Takemori, Chem. Mater. 16 (2004) 899–905.
[19] Z. Yu, J. Fan, B.Z. Tian, D.Y. Zhao, G.D. Stucky, Adv. Mater. 14 (2002) 1742–1745.
[20] H. Zhang, J.M. Sun, D. Ma, X.H. Bao, A. Klein-Hoffmann, G. Weinberg, D.S. Su, R. Schlçgl, J. Am. Chem. Soc. 126 (2004) 7440–7441.
[21] J.M. Sun, H. Zhang, R.J. Tian, D. Ma, X.H. Bao, D.S. Su, H.F. Zou, Chem. Commun. (2006) 1322–1324.
[22] H. Zhang, J.M. Sun, D. Ma, G. Weinberg, D.S. Su, X.H. Bao, J. Phys. Chem. B 110 (2006) 25908–25915.
[23] Y. Han, J.Y. Ying, Angew. Chem. Int. Ed. 44 (2005) 288–292;
Y. Han, J.Y. Ying, Angew. Chem. 117 (2005) 292–296.
[24] L. Cao, M. Kruk, J. Colloid Interface Sci. 361 (2011) 472–476.
[25] H.I. Lee, J.H. Kim, G.D. Stucky, Y. Shi, C. Pak, J.M. Kim, J. Mater. Chem. 20 (2010) 8483–8487.
[26] J. Sun, X. Bao, Chem. Eur. J. 14 (2008) 7478–7488.

[27] P. Van Der Voort, P.I. Ravikovitch, K.P. De Jong, A.V. Neimark, A.H. Janssen, M. Benjelloum, E. Van Bavel, P. Cool, B.M. Weckhuysen, E.F. Vansant, Chem. Commun. (2002) 1010–1011.
[28] P. Van Der Voort, P.I. Ravikovitch, K.P. De Jong, M. Benjelloum, E. Van Bavel, A.H. Janssen, A.V. Neimark, B.M. Weckhuysen, E.F. Vansant, J. Phys. Chem. B 106 (2002) 5873–5877.
[29] E. Van Barel, P. Cool, K. Aerts, E.F. Vansant, J. Phys. Chem. B 108 (2004) 5263–5268.
[30] V. Meynen, P. Cool, E.F. Vansant, Microporous Mesoporous. Mater. 104 (2007) 26–38.
[31] Z.Y. Wu, H.J. Wang, T.T. Zhuang, L.B. Sun, Y.M. Wang, J.H. Zhu, Adv. Funct. Mater. 18 (2008) 82–94.
[32] N. Lin, J.Y. Yang, Z.Y. Wu, H.J. Wang, J.H. Zhu, Microporous Mesoporous Mater. 139 (2011) 130–137.
[33] B.-H. Min, E.-Y. Jeong, M. Thommes, S.-E. Park, Chem. Commun. 47 (2011) 4673–4675.
[34] J. Heveling, C.P. Nicolaides, M.S. Scurrell, Appl. Catal. A 173 (1998) 1–9.
[35] M. Lallemand, A. Finiels, F. Fajula, V. Hulea, Appl. Catal. A 301 (2006) 196–201.
[36] M. Lallemand, O.A. Rusu, E. Dumitriu, A. Finiels, F. Fajula, V. Hulea, Appl. Catal. A 338 (2008) 37–43.
[37] J. Heveling, A. van der Beek, M. de Pender, Appl. Catal. 42 (1988) 325–336.
[38] B. Nkosi, F.T.T. Ng, G.L. Rempel, Appl. Catal. A 158 (1997) 225–241.
[39] F.T.T. Ng, D.C. Creaser, Appl. Catal. A 119 (1994) 327–339.
[40] V. Hulea, F. Fajula, J. Catal. 225 (2004) 213–222.
[41] S. Lin, L. Shi, M.M.L. Ribeiro Carrott, P.J.M. Carrott, J. Rocha, M. Li, X. Zou, Microporous Mesoporous Mater. 142 (2011) 526–534.
[42] J.C. Groen, T. Bach, U. Ziese, A.M. Paulaime-van Donk, K.P. de Jong, J.A. Moulijn, J. Pérez-Ramírez, J. Am. Chem. Soc. 127 (2005) 10792–10793.
[43] J.C. Groen, J.C. Jansen, J.A. Moulijn, J. Pérez-Ramírez, J. Phys. Chem. B 108 (2004) 13062–13065.
[44] J.C. Groen, J.A. Moulijn, J. Pérez-Ramírez, Microporous Mesoporous Mater. 87 (2005) 153–161.
[45] J.C. Groen, W. Zhu, S. Brouwer, S.J. Huynink, F. Kapteijn, J.A. Moulijn, J. Pérez-Ramírez, J. Am. Chem. Soc. 129 (2007) 355–360.
[46] R. Mokaya, W. Jones, Chem. Commun. (1998) 1839–1840.
[47] B.P. Feuston, J.B. Higgins, J. Phys. Chem. 98 (1994) 4459–4462.
[48] L. Shi, Y. Xu, N. Zhang, S. Lin, X. Li, P. Guo, X. Li, J. Solid State Chem. 203 (2013) 281–290.
[49] M. Kruk, M. Jaroniec, S.H. Joo, R. Ryoo, J. Phys. Chem. B 107 (2003) 2205–2213.
[50] B.L. Meyers, T.H. Fleisch, G.J. Ray, J.T. Miller, J.B. Hall, J. Catal. 110 (1988) 82–95.
[51] M. Tromp, J.A. van Bokhoven, M.T. Garriga Oostenbrink, J.H. Bitter, K.P. de Jong, D.C. Koningsberger, J. Catal. 190 (2000) 209–214.
[52] R. Giudici, H.W. Kouwenhoven, R. Prins, Appl. Catal. A 203 (2000) 101–110.
[53] J. Vernimmen, M. Guidotti, J. Silvestre-Albero, E.O. Jardim, M. Mertens, O.I. Lebedev, G. Van Tendeloo, R. Psaro, F. Rodriguez-Reinoso, V. Meynen, P. Cool, Langmuir 27 (2011) 3618–3625.
[54] E. Van Bavel, V. Meynen, P. Cool, K. Lebeau, E.F. Vansant, Langmuir 21 (2005) 2447–2453.
[55] M. Lallemand, A. Finiels, F. Fajula, V. Hulea, Stud. Surf. Sci. Catal. 170 (2007) 1863–1869.
[56] M. Shakeri, R.J.M. Klein Gebbink, P.E. De Jongh, K.P. De Jong, Microporous Mesoporous Mater. 170 (2013) 340–345.
[57] V. Hulea, F. Fajula, J. Catal. 225 (2004) 213–222.
[58] M. Lallemand, A. Finiels, F. Fajula, V. Hulea, J. Phys. Chem. C 113 (2009) 20360–20364.